Separation and Purification Technology 232 (2020) 115967

Contents lists available at ScienceDirect

Separation and Purification Technology

journal homepage: www.elsevier.com/locate/seppur

The oxidative degradation of diclofenac using the activation of peroxymonosulfate by $BiFeO_3$ microspheres—Kinetics, role of visible light and decay pathways

Fuman Han, Xin Ye, Qian Chen, Huimin Long, Yongfang Rao*

Department of Environmental Science and Engineering, Xi'an Jiaotong University, Xi'an 710049, PR China

ARTICLE INFO

Keywords:
$BiFeO_3$
Peroxymonosulfate
Degradation kinetics
Photocatalysis
Decay pathways

ABSTRACT

$BiFeO_3$ (BFO) microspheres were synthesized by a microwave-assisted hydrothermal method for the first time. The as-prepared BFO was comprehensively characterized by X-ray diffraction (XRD), X-ray photoelectron spectroscopy (XPS), scanning electron microscopy (SEM) and Mössbauer spectroscopy. The synthesized BFO was used to activate peroxymonosulfate (PMS) for the decomposition of diclofenac (DCF) in aqueous solution. DCF degradation was found to follow double-exponential decay kinetics in the BFO/PMS system. The effects of several operating parameters such as pH value, BFO dosage and PMS concentration on DCF degradation by BFO/PMS process were investigated in detail. Visible (Vis) light irradiation was observed to promote the DCF degradation by BFO/PMS process by producing additional sulfate and hydroxyl radicals and accelerating the Fe^{III}-Fe^{II}-Fe^{III} redox cycle. Both sulfate radicals ($SO_4^{\cdot -}$) and hydroxyl radicals ($^{\cdot}OH$) were detected in the BFO/PMS system by electron spin resonance (ESR). The reusability of as-prepared BFO microspheres was evaluated in both the BFO/PMS and the Vis/BFO/PMS systems. Nine intermediates were identified during DCF degradation in the BFO/PMS system and DCF decay pathways were proposed accordingly.

1. Introduction

Pharmaceuticals have incurred increasing concerns as emerging contaminants in recent years. A typical example is diclofenac (DCF), one of the most widely reported environmental pharmaceutical contaminants [1], due to its wide availability and the inefficiency of conventional treatment methods currently applied in WWTPs (Wastewater treatment plants) to remove DCF. DCF was frequently detected in groundwater [2,3] and surface water [4–6], although it is prone to natural photolysis. Even at environmentally relevant concentrations, DCF exerts adverse effects on different organisms [7–9]. The persistence of DCF in ecosystems and its potential toxicity towards various aquatic organisms have led to a rising interests in the development of effective treatment technologies for DCF.

Advanced oxidation processes (AOPs) have been proven to be an effective alternative to conventional treatment methods for the removal of PPCPs (pharmaceuticals and personal care products) in aqueous phase. The application of various AOPs, such as ozonation [10], photocatalysis [11], non-thermal plasma [12], sonication [13], photoelectrocatalysis [14] and irradiation [15] to remove DCF has been extensively studied. However, these AOPs have their drawbacks. Ozonation needs an intricate ozone generation system while other processes require continuous energy input. In recent years, sulfate radical-based AOPs (SRAOPs) have gained intensive interest as a desirable method to degrade pharmaceuticals [16], endocrine disruptors [17], and perfluorinated compounds [18] in water since the sulfate radical has a redox potential comparable to the hydroxyl radical while having a much longer half-life [19]. Compared to other SRAOP activation systems, such as UV, ultrasound, or microwave activation, the transition metal-activation based processes are more economical and less complicated in system configuration [20]. Metal-activation based systems can be either homogeneous or heterogeneous. Since heterogeneous catalysts can be recycled, they are the preferred method to activate PMS [20]. Cobalt oxide is one of the most popular catalysts to activate PMS for its high efficiency [21]. However, Co leaching from the catalysts causes health concerns due to its potential toxicity. Thus, the development of effective, stable and benign catalysts to activate PMS is still a challenge for practical application.

Perovskite oxides, (ABO_3 or A_2BO_4), characterized by their structural stability, elemental abundance and flexible chemical composition, are promising catalysts for various reactions [22,23]. Duan et al. reported that the catalytic activity of $Ba_{0.5}Sr_{0.5}Co_{0.8}Fe_{0.2}O_{3-\delta}$ (BSCF)

* Corresponding author.
E-mail address: yfrao@mail.xjtu.edu.cn (Y. Rao).

https://doi.org/10.1016/j.seppur.2019.115967
Received 14 June 2019; Received in revised form 20 August 2019; Accepted 20 August 2019
Available online 21 August 2019

perovskite toward PMS activation is much higher than that of a Co_3O_4 nanocatalyst [24]. In our previous study, $LaFeO_3$ exhibited significantly higher catalytic activity than Fe_2O_3 for activating PMS. $LaFeO_3$ catalyzed PMS for DCF degradation with a TOF (Turnover frequency) 17-fold higher than that of Fe_2O_3 [25]. However, in both studies, leaching of metal ions (Co^{2+} and La^{3+}) was observed, especially under acidic conditions. In recent years, Bismuth ferrite ($BiFeO_3$, BFO) has received increasing interests as a heterogeneous catalyst due to its multiferroic properties and high chemical stability, i.e., strong acid and alkali resistance [26–33]. In a previous study [34], BFO showed higher stability than $LaFeO_3$ did at pH 5.0; A significant amount of dissolved La (5.6 mg/L) was detected, while the concentration of dissolved Bi was only 5×10^{-4} mg/L with BFO and $LaFeO_3$ dosages of 1.0 g/L. Soltani and Lee also reported the stability of BFO during the catalytic degradation of 2-chlorophenol by BFO/PS or BFO/H_2O_2 [32].

Therefore, BFO/PMS process was used to remove DCF in the aqueous phase in the present study. BFO was prepared by a microwave-assisted hydrothermal method and comprehensively characterized. The catalytic activity of BFO towards PMS, H_2O_2 and PS activation was evaluated. The effects of diverse parameters including reaction pH levels, catalyst dosage, and PMS concentration on DCF decomposition were examined. The effect of visible light irradiationon DCF degradation in the BFO/PMS system was also investigated. The possible reaction mechanisms were unveiled. The intermediates/products were analyzed, and possible decay pathways of DCF were proposed.

2. Experimental

2.1. Materials

Bismuth nitrate pentahydrate ($Bi(NO_3)_3{\cdot}5H_2O$), iron nitrate nonahydrate ($Fe(NO_3)_3{\cdot}9H_2O$), sodium carbonate (Na_2CO_3) and potassium hydroxide (KOH) were purchased from Sinopharm Chemical Reagent Co., Ltd, China. Diclofenac (2-[2,6-dichlorophenyl]-amino]-benzene acetic acid sodium salt), 2, 6-dichloroaniline, Oxone, ethanol and tert-butanol from Sigma-Aldrich were employed in this study. All reagents are in analytic purity or higher and used without further purification.

2.2. Catalyst synthesis

The perovskite BFO was prepared by a microwave-assisted hydrothermal method. Bismuth nitrate and ferric nitrate were dosed into 10 mL deionized (DI) water with a molar ratio of 1:1. The mixture was stirred for 1 h in ambient air as the precursor of $BiFeO_3$. Then, sodium carbonate (Na_2CO_3) and potassium hydroxide (KOH) were added into the precursor solution as mineralizers. The obtained solution was heated in a 500 W microwave oven with the frequency of 2450 Hz at constant temperature (140 °C) for 35 min. After cooling, the particles were washed several times with Milli-Q water and dried at 80 °C for 12 h. The resulting product was finally ground into fine powders for further characterization.

2.3. Characterization of as-prepared BFO

The crystalline structure of BFO was determined by using an X-ray diffractometer at a scanning rate of 0.017° min^{-1} ranging from 20° to 80° (XRD, PANalytical Corp., Netherlands). The morphology of $BiFeO_3$ was obtained by the scanning electron microscopy conducted on the JEOL 2010 instrument with an accelerating voltage of 100 kV (SEM JEOL Corp., Japan). The surface chemical composition and chemical state of catalyst was determined using X-ray photoelectron spectroscopy (XPS, AXIS ULtrabld, Kratos). The 298 K Mössbauer spectrum was recorded on a Wissel Wss-10. The velocity drive transducer operated in a triangular waveform mode over energy ranges of ± 16 mm/s, with a 20 mCi ^{57}Co source dispersed as 10% in a thin Rh foil. The Brunauer–Emmett–Teller (BET) surface area of $BiFeO_3$ was investigated from N_2 adsorption/desorption isotherms at 77 K using an ASAP 2020 automatic analyzer (Micromeritics Instrument Corp., Norcross, GA, USA). UV–Vis absorption spectra were analyzed by an UV–Vis spectrophotometer (U-3010, HITACHI, Japan). The Zeta potentials of samples were obtained on a Brookhaven Zetasizer Nano ZS90Plus.

2.4. Catalytic reactions with and without visible light

All degradation experiments without visible light were carried out at room temperature in 100 mL of reaction solution. The DCF stock solution (0.2 mM) and PMS (0.1 M) were prepared in deionized water. The simulated wastewater with a concentration of 0.025 mM was obtained by adding predetermined aliquots of the DCF stock solution into DI water in the reactors. The as-synthesized BFO powder was added into DCF solution and the suspension was sonicated for 10 min. After 1 h stirring of suspension, adsorption equilibrium was reached (See Fig. S2b). Then, the catalytic reactions were started by dispensing PMS stock solution with predetermined volume into the reactor. Tetraborate was used to maintain the pH level during the catalytic reaction. Samples were filtered through a poly(tetrafluoroethylene) (PTFE) membrane of 0.2 μm pore size. The reactions were quenched by sodium thiosulfate ($Na_2S_2O_3$). In the case of photocatalytic reactions, a 420 nm LED was used as light source. All experiments were performed in duplicate.

2.5. Analytic methods

The remaining DCF after reaction was quantified by high-performance liquid chromatography (HPLC). Possible cation leaching (Bi and Fe) was detected by ICP (Inductively coupled plasma) (ICPE-9000, SHIMADZU).

Liquid chromatography/electrospray-time-of-flight mass spectrometry (UPLC/ESI-TOF-MS), was applied to identify the intermediates/products obtained from diclofenac decomposition. Separation was performed by Waters UPLC system (ACQUITY UPLC I-Class) equipped with a reverse-phase 2.1 mm × 50 mm C18 analytical column and 1.7 μm particle size (Waters ACQUITY UPLC-BEH C18). SPME (Solid phase microextraction)/GC/MS was also employed to determine the degradation intermediates/products. The detailed procedure was presented in a previous study [35].

Electron spin resonance (ESR) spectrometer (Bruker EMXPLUS6/1) was used to identify the active species in BFO/PMS system using DMPO (5, 5-dimethyl-pyrroline N-oxide) as the spin trapping agent. DMPO stock solution was added to catalytic reaction solution to obtain the final concentration of 88 mM.

3. Results and discussion

3.1. Characterization of $BiFeO_3$

The XRD pattern of as-prepared sample confirmed the formation of pure-phase BFO as shown in Fig. S1. The characteristic peaks at 2θ of 22.5°, 31.8°, 32.1°, 39.0°, 39.5°, 45.9°, 51.5°, 56.5°, 57.0°, 66.4°, 67.1°, 70.6°, 71.7° and 76.1° correspond to 012, 104, 110, 006, 202, 024, 122, 018, 214, 208, 220, 036, 312 and 134 planes of BFO (JCPDS No. 71-2494). All diffraction peaks can be indexed on the basis of a rhombohedral structure with space group R3c. The following lattice parameters were determined: a = b = 5.57 Å and c = 13.85 Å.

The XPS was utilized to further identify the chemical state and composition of the as-prepared BFO samples Fig. 1a showed the survey spectrum and high-resolution spectra of Bi 4f, Bi 4p, Bi 4d, Bi 5d, Fe 2p and O 1s orbitals, which confirmed the existence of Bi, Fe, and O elements. The observed peak for C 1s is probably ascribed to adventitious carbon in air. For the spectrum of Bi 4f (See Fig. 1b), the peaks at 163.3 eV and 158.1 eV corresponding to the Bi $4f_{5/2}$ and Bi $4f_{7/2}$ orbital suggests the presence of Bi^{3+} [36–38]. As shown in Fig. 1c, the two

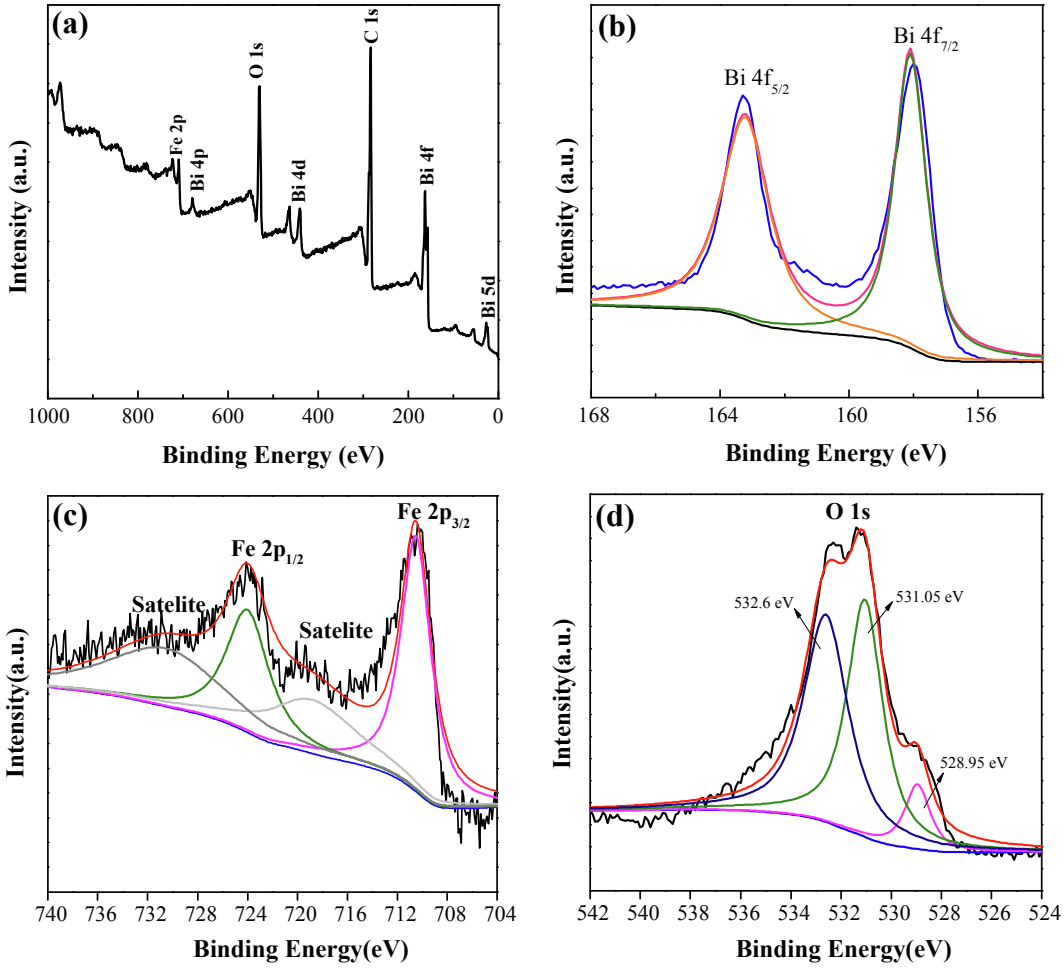

Fig. 1. XPS spectra of as-prepared BFO: (a) Survey spectrum; (b) Bi 4f; (c) Fe 2p and (d) O 1s.

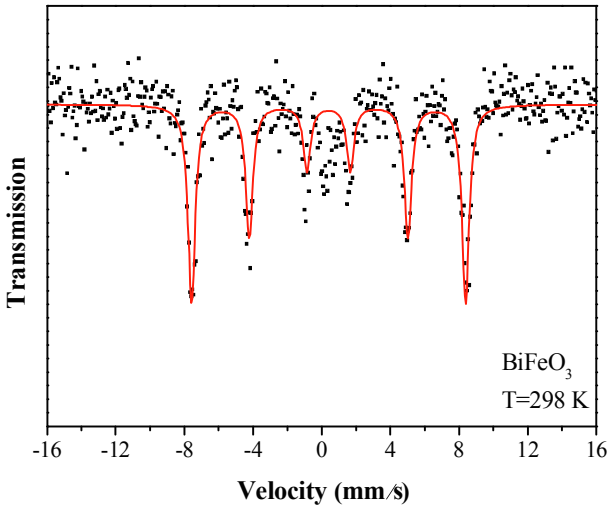

Fig. 2. The room-temperature transmission ^{57}Fe Mossbauer spectra of BFO.

peaks at binding energies of 724.1 and 710.5 eV can be assigned to the Fe $2p_{1/2}$ and Fe $2p_{3/2}$, respectively. The satellite peak at 719.0 was found about 8.5 eV above the Fe $2p_{3/2}$ peak, suggesting Fe exists as Fe^{3+} in the as-prepared BFO [36,39]. Furthermore, another satellite peak at 730.5 eV may be the satellite peak for Fe $2p_{1/2}$ [39]. The oxidation state of Fe is important for the reaction mechanism of PMS activated by BFO. Mössbauer spectroscopy was used to further confirm the oxidation state of Fe. Fig. 2 shows the room-temperature transmission ^{57}Fe Mössbauer spectra of BFO. It exhibits a six-line magnetic hyperfine pattern with an isomer shift (IS) of 0.402 mm/s. The six-line magnetic hyperfine pattern is characteristic of magnetically ordered Fe^{3+} moments [40]. In addition, the IS reflects the s-electron density at the iron nucleus, which is very sensitive to the oxidation state of Fe. Fe^{3+} usually shows an IS in the range 0.3–0.6 mm/s while the IS of Fe^{2+} is within the range 0.7–1.2 mm/s [41]. Thus, it can be concluded that the oxidation state of Fe is +3 and no Fe^{2+} exists in the as-prepared BFO. Fig. 1d shows O 1s peak, which can be deconvolved into three separate peaks located at 528.9, 531.0 eV and 532.5 eV, which are associated with lattice O, the O in hydroxyl groups and the O in adsorbed H_2O on the surface of BFO, respectively [42,43].

The microscopic homogeneity of the BFO is investigated using SEM. As shown in Fig. 3a, the BFO particles exhibit well-dispersed microspheres ranging from 10 to 20 μm. Fig. 3b further confirms the BFO particles are roughly spherical and the microspheres are believed to result from the agglomeration of irregular segments.

The BET specific surface area of as-prepared BFO was measured to be 2.5 m^2/g by their N_2 adsorption/desorption isotherms. The relatively small BET specific surface area may be ascribed to the speed of crystallization leading to crystal agglomeration (See Fig. 3b).

3.2. Catalytic activity of BFO toward different oxidant

PMS, $S_2O_8^{2-}$ and H_2O_2 are common oxidants widely used in wastewater treatment. It has been reported BFO can activate H_2O_2 [34] and $S_2O_8^{2-}$ [33] for the degradation of organic pollutants. In order to

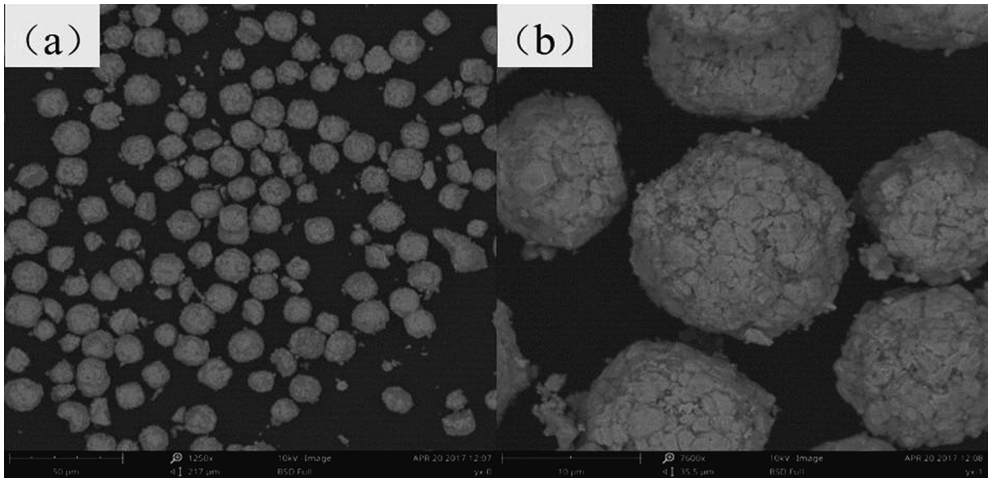

Fig. 3. SEM photographs of as-prepared BFO.

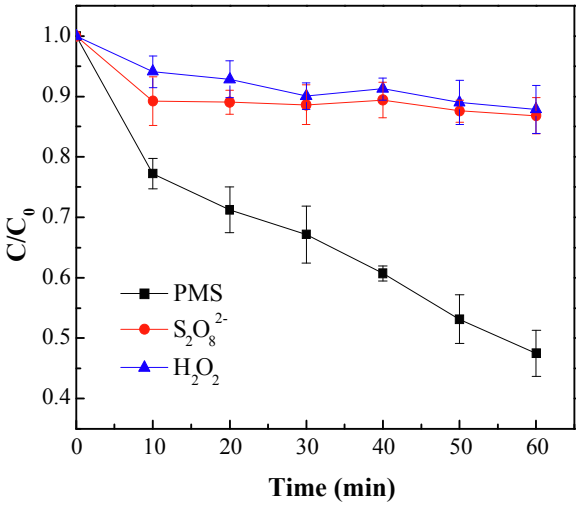

Fig. 4. DCF degradation by different BFO-catalyzed oxidants (Notes: $[DCF]_0$ = 0.025 mM, BFO dosage = 0.3 g/L, [PMS] = $[S_2O_8^{2-}]$ = $[H_2O_2]$ = 0.5 mM, tetraborate buffered pH 7.0).

compare the catalytic activity of BFO toward different oxidants, DCF degradation was investigated in BFO/H_2O_2, BFO/ $S_2O_8^{2-}$ and BFO/ PMS systems. No DCF degradation was observed for the sole-PMS system and sole-BFO system (See Fig. S2). The adsorption of DCF on BFO surface was around 10% (See Fig. S2). All reactions were conducted at neutral pH level. As shown in Fig. 4, DCF degradation was insignificant in both the BFO/$S_2O_8^{2-}$ and the BFO/ H_2O_2 system. The activation of PMS by BFO removed 47% of DCF in 60 min. There is a hydrogen atom on the one side of O—O bond of PMS. The $S_2O_8^{2-}$ ion has 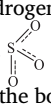 on the both sides of O—O bond, implying that the O—O bond of $S_2O_8^{2-}$ is more difficult to activate in comparison with that of PMS due to steric effects. In the case of H_2O_2, the O—O bond length in H_2O_2 (1.453 Å) is shorter than that in HSO_5^- (1.460 Å) [44], suggesting that the O—O bond in HSO_5^- more easily broken. Therefore, the BFO/PMS process was selected for DCF degradation for further study.

The degradation reaction of organic compounds commonly follows pseudo-first-order kinetics in heterogeneous Fenton-like systems. However, first-order kinetics did not fit the DCF degradation process (R^2 of 0.79) in the BFO/PMS system; neither could Zero-order and second-order kinetics. Wang et al. reported a similar phenomenon in their study [29]. They found the degradation of bisphenol A in the presence of EDTA (Ethylenediaminetetraacetic acid) can be fitted to a triple exponential expression. In this study, DCF decay curve can be well fitted to a double exponential expression as described below (Eq. (1), R^2 = 0.997):

$$\frac{C_t}{C_0} = a_1 e^{-k_1 t} + a_2 e^{-k_2 t} \quad (1)$$

where C_t and C_0 is the DCF concentration (mM) at reaction time of t and 0, respectively; a_1 and a_2 represent fraction coefficients while k_1 and k_2 are apparent rate constants (min^{-1}) for the 1st type and 2nd type of DCF degradation, respectively. This may imply that DCF's overall degradation consists of two separate concurrent pseudo-first-order catalytic processes with different decay rates in the BFO/PMS system. Based on the study of Wang et al., the two separate catalytic processes can be assumed to happen at non-occupied active sites and competitive sites, respectively. Non-occupied active sites indicate ones available for DCF degradation on the surface of fresh BFO microspheres while competitive sites are ones which DCF and the generated intermediates compete for. The two types of catalytic reaction are assumed to occur simultaneously, suggesting $a_1 + a_2 = 1$. Based on a double exponential fitting, a_1 and a_2 were determined to be 0.26 and 0.74, respectively while k_1 and k_2 were 0.121 min^{-1} and 0.0055 min^{-1}, respectively. The fitting results indicate that DCF degradation at competitive sites is insignificant compared to that at non-occupied active sites and that further degradation is inhibited substantially by generated degradation products.

In order to evaluate the stability of BFO during the action of PMS, the BFO particles were recovered, washed and reused for 3 times. As shown in Fig. S3, no significant deactivation was observed for DCF degradation in BFO/PMS system during four cycles, where DCF removal efficiency declined from 52.5% for the first cycle to 49% for the fourth cycle. In addition, no Bi^{3+} or Fe^{3+} were detected during DCF degradation at pH 7.0 in the BFO/PMS system. These experimental results indicate that the as-prepared BFO has the potential to be employed in the real application of wastewater treatment.

3.3. Influence of pH level

The influence of pH levels ranging from 3.00 to 9.00 on DCF degradation was tested as shown in Fig. 5. The pH value shows significant effect on the performance of the BFO/PMS process. DCF degradation was found to fit Eq. (1) at all pH levels except at pH 9.0. The kinetic parameters based on double-exponential fittings are listed in Table S1. The fastest degradation rate of DCF was observed at pH 3.0. However, iron leaching from BFO at pH 3.0 was determined to be 0.15 mg/L after 1 h. Bismuth leaching was not detected. In order to identify the

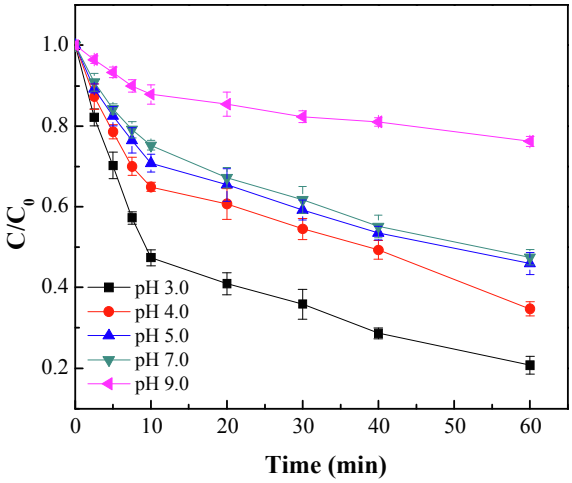

Fig. 5. Effects of pH level on DCF degradation (Notes: $[DCF]_0$ = 0.025 mM, $[BiFeO_3]$ = 0.3 g L^{-1}, $[PMS]_0$ = 0.5 mM).

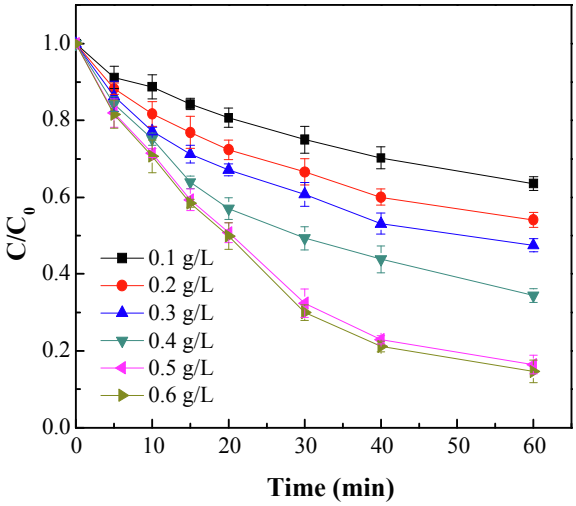

Fig. 6. Effects of BFO dosage on DCF degradation (Notes: $[DCF]_0$ = 0.025 mM, $[PMS]_0$ = 0.5 mM, tetraborate buffered pH 7.0).

contribution of the homogeneous reaction (activation of PMS by Fe^{3+}) for DCF elimination at pH 3.0, DCF degradation in Fe^{3+} (0.15 mg/L)/PMS system was investigated. As shown in Fig. S4, around 65.4% removal efficiency of DCF was achieved, suggesting homogeneous reaction made a significant contribution to DCF degradation at pH 3.0. The DCF degradation rate at pH 7.0 is similar to that at pH 5.0, but slower than that at pH 4.0. Both Bismuth and iron leaching was not observed in BFO/PMS system at pH above 4.0, indicating the wide pH range tolerance of as-prepared BFO microspheres. The degradation of DCF was substantially inhibited at pH 9.0. The pKa_1 of H_2SO_5 is less than 0 [45] and the pKa_2 is 9.4 [46], implying PMS exists in the form of HSO_5^- at pH ≤ 7 while HSO_5^- and a small portion of SO_5^{2-} are both present at pH 9.0. The pH_{pzc} of BFO was determined to be around 3.2 (See Fig. S5). When pH is above 4, the increase of negative surface charge may lead to the enhanced electrostatic repulsion between BFO and PMS species, especially SO_5^{2-}, at the elevated pH levels. And thus reduce the generation of sulfate radicals. In addition, it was reported that the p*K*a of DCF is 4.15 [47], implying that the DCF exist as an anion at pH above 4.15. The electrostatic repulsion prevented DCF anion from approaching the negatively-charged surface of BFO. Qi et al. reported that peroxymonosulfate could be activated by base for the degradation of some organic pollutants such as dye, phenol and bisphenol A [48]. However, it was not observed that basic conditions were favorable for the degradation of DCF in BFO/PMS system. In the study of Qi et al., the PMS/base system was effective for different organic compounds, while the degradation of 4-chlorophenol was insignificant. Thus, the activation of PMS by base may not significantly contribute to the degradation of DCF. Since PMS exists in the form of HSO_5^- and SO_5^{2-} at pH 9.0, electrostatic repulsion between the two species and the negatively-charged BFO surface prevented HSO_5^- and SO_5^{2-} from approaching BFO surface. Thus, DCF degradation was significantly retarded at pH 9.0.

3.4. Influence of BFO dosage and PMS concentration

At pH 3.0, iron leaching was observed as described above. At pH 4.0, the DCF degradation was only slightly faster than that at pH 7.0. Thus, the following studies were conducted at pH 7.0 considering the practical application of the BFO/PMS process. To study the influence of BFO dosage on the DCF degradation, BFO doses from 0.1 to 0.6 g/L were applied to activate PMS for DCF decomposition. As illustrated in Fig. 6 and Table S1, an enhanced DCF degradation rate was achieved by increasing the BFO dosage. It was also observed that the DCF degradation fit Eq. (1) with BFO dosages ranging from 0.1 to 0.4 g/L (See Table S1). The increase of BFO dosage resulted in the increase of a_1 and the decrease of a_2, indicating that the contribution of DCF degradation at competitive sites declined. It is interesting to note that DCF degradation followed pseudo first-order kinetics with a BFO dosage above 0.5 g/L with $R^2 > 0.97$. This may be because there are enough active sites on the BFO surface that the activation of PMS and DCF degradation at competitive sites is negligible. When BFO loading was increased from 0.5 to 0.6 g/L, the observed DCF decay rate constant slightly rose from 0.0332 to 0.0351 min^{-1}. Therefore, 0.5 g/L was selected as BFO dosage for further study.

DCF degradation was also investigated at varied PMS concentrations with a BFO dosage of 0.5 g/L. DCF degradation fit pseudo first-order kinetics with $R^2 > 0.93$. As shown in the inset of Fig. 7a, the linear increase of DCF degradation rate was observed with escalating PMS concentrations from 0.1 to 0.5 mM. When PMS concentration was continually increased to 0.6 mM, the enhancement of the DCF degradation constant is insignificant (Increasing from 0.0332 to 0.0358 min^{-1}). On the one hand, the chance of PMS diffusing to the surface of BFO increased with increasing PMS concentration, resulting in the more activation of PMS ions on the BFO surface. On the other hand, overdosing PMS can be a sink for sulfate radicals (Eq. (2)). As shown in Fig. 7b, around 81.3% of PMS (0.488 mM) remained in the reaction solution after 1 h with a initial concentration of PMS at 0.6 mM, which is not cost effective. The reaction stoichiometric efficiency (RSE) was also calculated for all PMS concentrations applied at different reaction times (10–60 min) as demonstrated in Fig. S6. The highest RSE (ranging from 16.6 to 23.1%) was obtained using 0.3 mM of PMS at the highest reaction time while the lowest RSE was observed at 0.1 mM of PMS. Therefore, the optimum PMS concentration is 0.5 mM in terms of reaction rate constant while the optimum PMS concentration is 0.3 mM in terms of RSE with a fixed BFO dosage of 0.5 g/L.

$$HSO_5^- + SO_4^{\cdot -} \rightarrow SO_5^{\cdot -} + SO_4^{2-} + H^+ \quad (2)$$

3.5. Influence of radical scavengers and identification of reactive species

ESR spectroscopy using DMPO as spin-trapping adduct were employed to identify the active species generated during the activation of PMS by BFO. Both characteristic peaks of DMPO-$SO_4^{\cdot -}$ and DMPO-$^{\cdot}$OH [49] adducts were observed in the BFO/PMS systems, implying the generation of $SO_4^{\cdot -}$ and $^{\cdot}$OH (See Fig. 8a). No signal was detected in the systems with PMS and BFO alone. Compared to DMPO-$SO_4^{\cdot -}$, the stronger peak intensities of DMPO-$^{\cdot}$OH might be ascribed to rapid transformation from DMPO-$SO_4^{\cdot -}$ to DMPO-$^{\cdot}$OH [50,51].

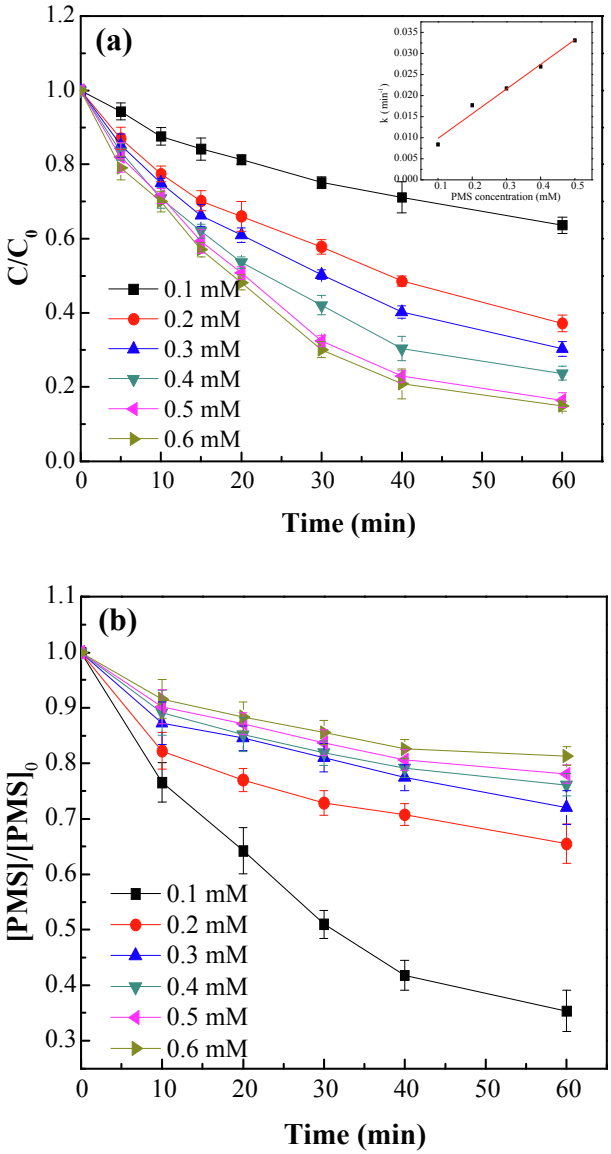

Fig. 7. (a) Effects of PMS concentration on DCF degradation; (b) PMS decomposition at different concentration (Notes: $[DCF]_0$ = 0.025 mM, [BFO] = 0.5 g/L, tetraborate buffered pH 7.0).

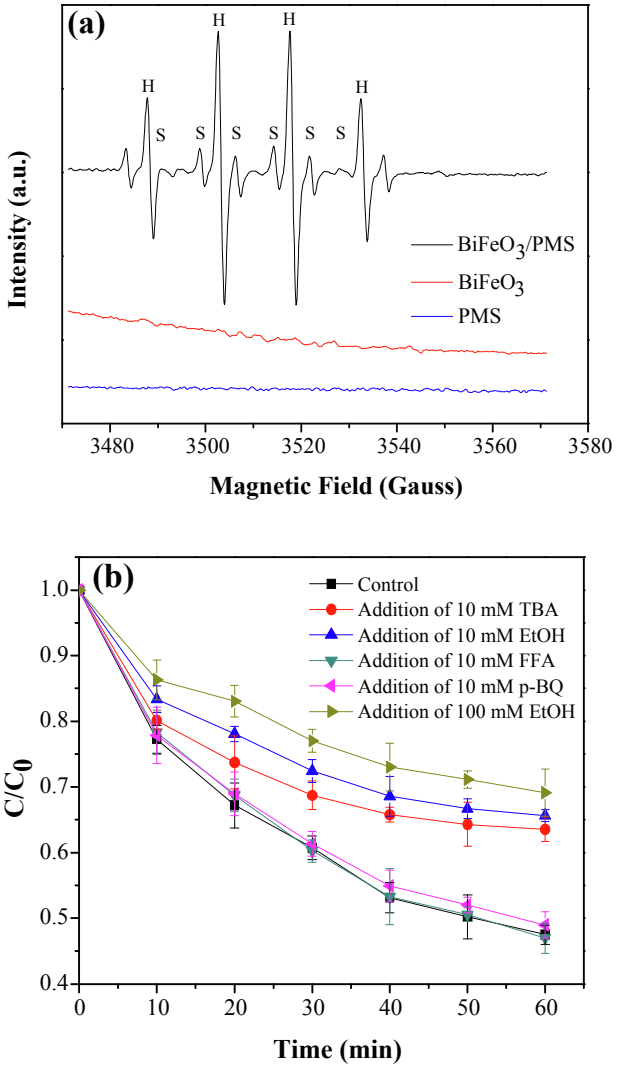

Fig. 8. (a) DMPO spin-trapping ESR spectra of BFO, PMS and BFO/PMS; (b) Effects of radical scavengers on DCF degradation; (Notes: $[DCF]_0$ = 0.025 mM, BFO dosage = 0.3 g/L, $[PMS]_0$ = 0.5 mM, tetraborate buffered pH 7.0).

In order to clarify the contribution of sulfate radicals and hydroxyl radicals to the degradation of DCF, two radical scavengers, i.e. ethanol and tert-butanol were added to the reaction solution. Ethanol is effective quencher for both sulfate radicals ($3.5–7.7 \times 10^7\ M^{-1}\ s^{-1}$) and hydroxyl radicals ($9.7 \times 10^8–1.9 \times 10^9\ M^{-1}\ s^{-1}$). Tert-butanol (t-BuOH) can only react with hydroxyl radicals rapidly ($3.8–7.6 \times 10^8\ M^{-1}\ s^{-1}$) while the reaction rate constant between t-BuOH and sulfate radical is around $(4–9.1) \times 10^5\ M^{-1}\ s^{-1}$ [52]. As demonstrated in Fig. 8b, the presence of 10 mM t-BuOH lowers the DCF removal efficiency from 52.5% to 36.4%. The inhibiting effect of 10 mM ethanol is slightly greater than that of t-BuOH, with DCF removal efficiency decreasing from 52.5% to 34%. Even in the presence of 100 mM ethanol, DCF removal efficiency still reached 29.8%. It was reported that the second-order reaction rate constant between the sulfate radical and DCF was around $(9.2 \pm 2.6) \times 10^9\ M^{-1}\ s^{-1}$ [53]. The bimolecular reaction rate constant for hydroxyl radical with DCF was reported to be $(2.45–9.29) \times 10^9\ M^{-1}\ s^{-1}$ [54,55]. The bimolecular reaction rate constants for ethanol with sulfate radicals and hydroxyl radicals are $(3.5–7.7) \times 10^7\ M^{-1}\ s^{-1}$ and $9.7 \times 10^8–1.9 \times 10^9\ M^{-1}\ s^{-1}$, respectively. The rate constant between DCF and sulfate radical is two orders of magnitude higher than that between ethanol and sulfate radical. The $k_{DCF,OH}$ and $k_{ethanol,OH}$ are nearly the same order of magnitude. The ethanol concentration (100 mM) is 4000 times the concentration of DCF (0.025 mM) and 200 times the concentration of PMS (0.5 mM). Theoretically, 100 mM ethanol is enough to scavenge the generated sulfate radicals and hydroxyl radicals. However, 100 mM ethanol failed to inhibit DCF degradation completely. Both ethanol and t-BuOH are hydrophilic compounds. Thus, it is difficult for them to accumulate on the BFO surface [56], leading to them mainly competing for the radicals in the bulk solution. On the other hand, the scavengers such as ethanol and methanol did not interfere with the interaction between metal oxides and PMS [25,57]. Thus, the quenching effect of scavengers would not be very significant if the surface-bound sulfate radicals and hydroxyl radicals made a major contribution to DCF degradation in BFO/PMS system.

Gao et al. reported that the activation of perovskite oxides including $LaFeO_3$, $LaZnO_3$, $LaMnO_3$ and $LaNiO_3$ could generate singlet oxygen. In their study, they also claimed singlet oxygen was the dominant ROS which was responsible for ofloxacin degradation [58]. It was also reported that singlet oxygen and superoxide radicals rather than sulfate and hydroxyl radicals are dominant contributors to the oxidation of organic pollutants including phenol and various dyes in the magnetic carbon supported Prussian blue nanocomposite Fe_3O_4@C/PB/PMS system [59]. In order to identify the role of singlet oxygen and superoxide radicals in DCF degradation by BFO/PMS process, the effect of

furfuryl alcohol (FFA) and p-benzoquinone (p-BQ) on DCF degradation was investigated. The p-BQ is an effective scavenger for superoxide radicals [59,60] while FFA is a singlet oxygen scavenger [61]. As shown in Fig. 8b, both FFA and p-BQ exerted no influence on DCF degradation, suggesting the role of singlet and superoxide radicals is insignificant in DCF degradation in the BFO/PMS system.

Based on our experimental results, the mechanisms of PMS activation by BFO is described in Eqs. (3)–(8). Firstly, a complex between $\equiv Fe^{III}$ and HSO_5^- was formed (Eq. (3)), where $\equiv Fe^{III}$ represents Fe^{3+} sites on BFO surface. The electron was transferred from HSO_5^- to $\equiv Fe^{III}$, leading to the generation of $\equiv Fe^{II}$ and $SO_5^{-\cdot}$ (Eq. (4)). The generated $\equiv Fe^{II}$ activated HSO_5^- to yield $SO_4^{-\cdot}$ and $\equiv Fe^{III}$ (Eq. (5)). The $SO_4^{-\cdot}$ can react with H_2O or OH^- to produce $HO^{\cdot}$ (Eqs. (6) and (7), respectively). The combination of $SO_5^{-\cdot}$ and $SO_5^{-\cdot}$ may also generate $SO_4^{-\cdot}$ (Eq. (8)) [62].

$$\equiv Fe^{III}–OH^- + HSO_5^- \rightarrow \equiv Fe^{III}–(OH)OSO_3^- + OH^- \quad (3)$$

$$\equiv Fe^{III}–(OH)OSO_3^- \rightarrow \equiv Fe^{II} + SO_5^{-\cdot} + H^+ \quad (4)$$

$$\equiv Fe^{II} + HSO_5^- \rightarrow \equiv Fe^{III} + SO_4^{-\cdot} + OH^- \quad (5)$$

$$SO_4^{-\cdot} + H_2O \rightarrow HO^{\cdot} + SO_4^{2-} + H^+ \quad (6)$$

$$SO_4^{-\cdot} + OH^- \rightarrow HO^{\cdot} + SO_4^{2-} \quad (7)$$

$$SO_5^{-\cdot} + SO_5^{-\cdot} \rightarrow SO_4^{-\cdot} + SO_4^{-\cdot} + O_2^{-\cdot} \quad (8)$$

The mechanisms for the heterogeneous activation of PMS or PS are complicated. In recent years, non-radical mechanisms were also proposed for heterogeneous activation of PMS or PS for the degradation of organic compounds [63–65]. Since an excess amount of ethanol could not completely inhibit DCF degradation in the BFO/PMS system, the contribution from non-radical pathways to DCF degradation might be significant and needs further investigation.

3.6. Photocatalytic degradation of DCF under visible light irradiation

BFO has been reported to be an effective visible-light photocatalyst due to its narrow band gap and stability [32]. In this study, the photocatalytic activity of BFO was investigated in terms of DCF degradation under the irradiation of 420 nm LED lamp with and without the presence of PMS. The optical property and energy band structure are believed to play a critical role in the photocatalytic activity of semiconductors. The UV–visible absorption spectra of BFO microspheres is demonstrated in Fig. S7, where the synthesized BFO microspheres exhibit strong absorption in the visible range. The band gap (Eg) of as-prepared BFO was calculated to be 1.89 eV using the $(\alpha h\nu)^2$ as a function of $h\nu$ (See Fig. S8). Furthermore, the valence band maximum (VBM) was determined to be 1.25 eV according to the valence band XPS analysis of BFO (Fig. S9). Based on the formula $E_{CBM} = E_{VBM} - Eg$, the conduction band minimum (E_{CBM}) was calculated to be −0.64 eV.

As shown in Fig. 8, BFO microspheres failed to exhibit any photocatalytic activity under visible light irradiation. The E_{CBM} (−0.64 eV) and E_{VBM} (1.25 eV) of as-prepared BFO microspheres indicate that the photogenerated electrons on the CB of BFO can reduce O_2 to $O_2^{\cdot -}$ and the holes cannot oxidize H_2O to generate hydroxyl radicals on the VB of BFO. $E_0(O_2/O_2^{\cdot -})$ and $E^0(^{\cdot}OH/H_2O)$ are −0.33 eV and 2.37 eV, respectively[66]. The oxidizing power of $O_2^{\cdot -}$ may not be strong enough for the oxidation of DCF. In addition, the fast recombination of the electron and hole pair may be expected due to the narrow band gap of BFO. Under the irradiation of visible light (420 nm), PMS could not be activated to degrade DCF (See Fig. 9). Nevertheless, the irradiation of visible light promoted the DCF decomposition by BFO/PMS noticeably, where the removal efficiency of DCF increased from 52.5 to 68.0%. This is because the photogenerated electrons on the CB of BFO can reduce PMS to yield more hydroxyl radicals or sulfate radicals (Eqs.9 and 10). This experimental result (See Fig. S10) can further prove the reduction of PMS by photogenerated electrons. In addition, the photogenerated

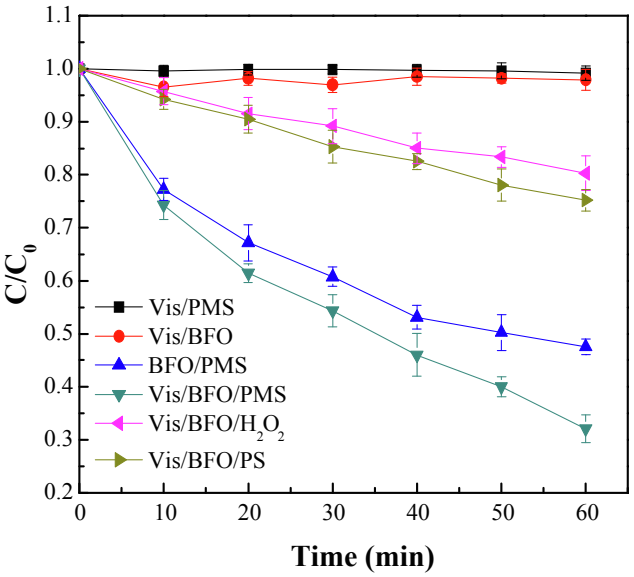

Fig. 9. Photocatalytic degradation of DCF with and without PMS (Notes: $[DCF]_0$ = 0.025 mM, BFO dosage = 0.3 g/L, [PMS]0 = $[H_2O_2]$ = [PS] = 0.5 mM, tetraborate buffered pH 7.0).

electrons and $O_2^{\cdot -}$ could reduce Fe(III) to Fe (II), accelerating the Fe^{III}-Fe^{II}-Fe^{III} redox cycle and thus promoting the generation rate of sulfate radicals (Eqs. (11)–(13)).

$$HSO_5^- + e_{CB}^- \rightarrow SO_4^{\cdot -} + OH^- \quad (9)$$

$$HSO_5^- + e_{CB}^- \rightarrow {}^{\cdot}OH + SO_4^{2-} \quad (10)$$

$$\equiv Fe^{III} + e_{CB}^- \rightarrow \equiv Fe^{II} \quad (11)$$

$$\equiv Fe^{III} + O_2^{\cdot -} \rightarrow \equiv Fe^{II} + O_2 \quad (12)$$

$$\equiv Fe^{II} + HSO_5^- \rightarrow \equiv Fe^{III} + SO_4^{\cdot -} + OH^- \quad (13)$$

The influence of visible light on DCF degradation in the BFO/H_2O_2 and Vis/BFO/PS systems has also been investigated. As shown in Figs. 4 and 9, visible light irradiation increased DCF removal efficiency from roughly 10% to 20% and 25% in the BFO/H_2O_2 and Vis/BFO/PS system, respectively.

The reusability of BFO for DCF degradation in Vis/BFO/PMS system has also been tested. As demonstrated in Fig. S11, no significant decline (from 68% to 65%) in DCF removal efficiency was observed during four cycles. No Bi and Fe leaching was detected during DCF degradation in Vis/BFO/PMS system. These results suggest that the as-prepared BFO catalyst is stable and can be recycled for the degradation of organic pollutants in the Vis/BFO/PMS system.

3.7. Identification of DCF degradation intermediates and degradation pathways

The degradation of DCF shared the same intermediates in the UV/BFO/PMS and BFO/PMS systems. This is because DCF degradation relied on the oxidation of sulfate radicals and hydroxyl radicals in both processes. Visible light irradiation offered an additional way to produce hydroxyl and sulfate radicals and promoted the Fe^{III}-Fe^{II}-Fe^{III} redox cycle. Visible light irradiation did not change the dominating DCF degradation mechanism which is the oxidation of hydroxyl and sulfate radicals. Nine intermediates were detected and identified by Liquid chromatography/electrospray-time-of-flight mass spectrometry (LC/ESI-TOF-MS) and Gas Chromatography-Mass Spectrometer (GC-MS). Molecular structure of each intermediate/product is shown in Table S2 and MS spectra are shown in supplementary data.

Among these intermediates, compound 1 with a *m/z* of 160.97 was

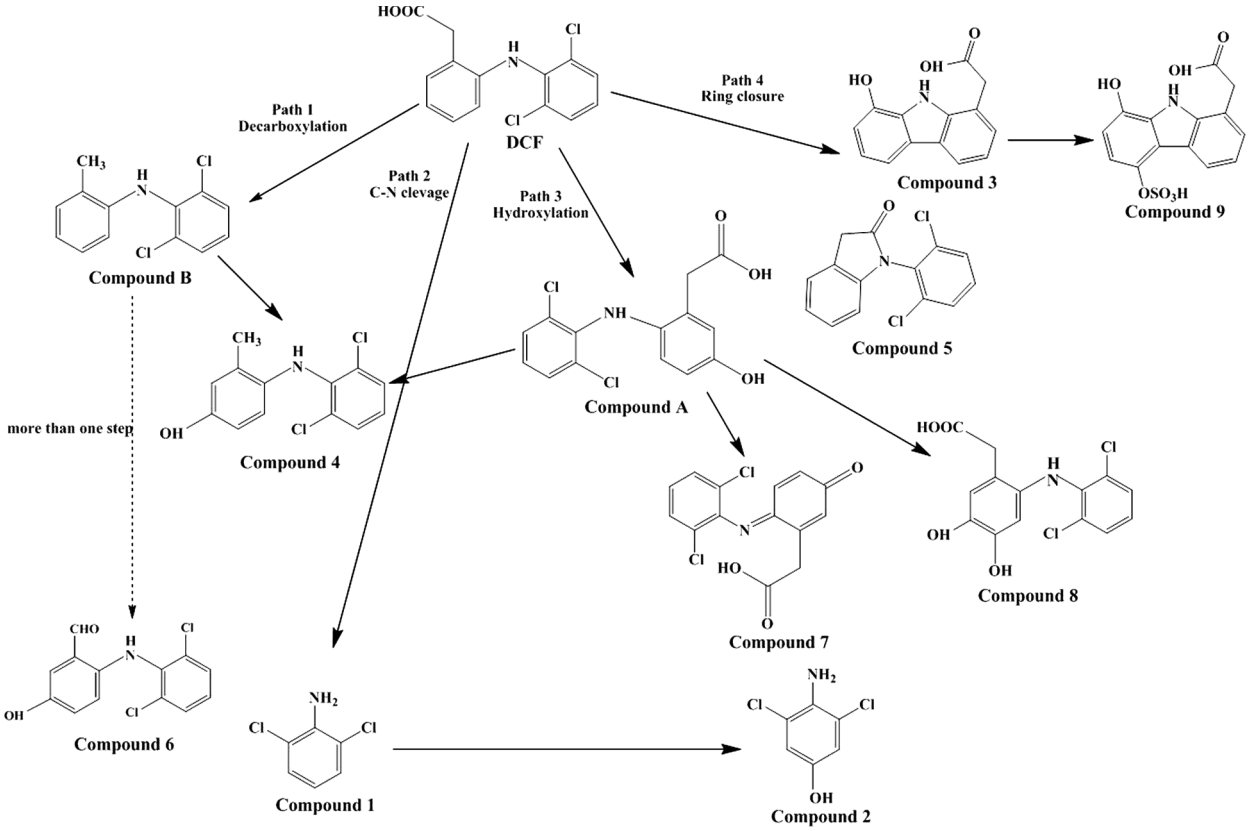

Fig. 10. Possible decay pathways of DCF in BFO/PMS system.

detected during the whole DCF degradation process. It was also detected in previous studies [67–71]. The fragment *m/z* 145.00 and 125.92 corresponds to the loss of $-NH_2$ and $-Cl$, respectively. Compound 1 was identified as 2,6-dichloroaniline, which was confirmed by the comparison of the retention time and MS patterns of compound 1 and the standard compound. Compound 2 was also a major intermediate showing a *m/z* of 177.95. The fragment *m/z* 141.96 was the result of dechlorination. MS spectra of compound 3 shows two fragments *m/z* 228.2312 and 214.2510 resulting from the loss of group −NH and −CO respectively. In the case of compound 4 (*m/z* = 267.01), the *m/z* 237.18 fragment corresponds to the loss of $-CH_3$ and −OH and the *m/z* 105.05 fragment may be generated by the broken of C-N bond. Compound 5 was identified by both GC-MS (*m/z* = 277.11), and LC-MS ($[M+H]^+$ = 278.0128). The fragment *m/z* 250.0188 is believed to come from the loss of −CO. Compound 6 is believed to derive from the oxidation of compound 4. A fragment with *m/z* 265.01 corresponds to −OH loss of compound 6 (*m/z* = 281.01). Compound 7, with a $[M+H]^+$ of 310.0017, is a quinone-like intermediate product which was also observed in previous studies [10,11,70,72]. The fragment *m/z* 291.9909 came from an 18 Da loss ($-H_2O$) of *m/z* 310. The compound 8 is a typical hydroxylation product [11,68,73]with a $[M+H]^+$ of 327.0766 in this study. The benzene ring of compound 3 was attacked by sulfate radical, leading to the generation of Compound 9 which was reported in previous studies [25,74].

The possible decay pathways of DCF in BFO/PMS system were proposed. As shown in Fig. 10, there are four primary pathways for DCF degradation. In reaction pathway 1, DCF was decarboxylated to yield 2,6-dicloro-N-o-tolylbenezamine (Compound B), which was transformed to compound 6 by the oxidation of methyl and hydroxylation on the left benzene ring. The further hydroxylation of compound B generated compound 4. In reaction pathway 2, dichloroaniline (Compound 1), which is the main product, was obtained by a C−N bond cleavage process. Compound 1 could also be derived from compounds A, B, 4, 6 and 8. Pathway 3 is the hydroxylation of DCF. The hydroxylated diclofenac derivative 5-hydroxy-diclofenac (Compound A) could be further transformed to (2-(2, 6-dichlorophenylamino) phenyl) methanol (Compound 4), diclofenac-2,5-iminoquinone (Compound 7) and 4,5-dihydroxy-diclofenac (Compound 8) through decarboxylation, dehydrogenation and hydroxylation processes, respectively. In reaction pathway 4, the (2,6-dichlorophenyl)-indolin-2-one was formed by ring closure with the loss of H_2O. Furthermore, another ring closure pathway might proceed through a multistep process including dechlorination (the C−Cl bond could be attacked by $SO_4^{\cdot -}$ or other substances [75]), hydroxylation and ring closure reactions to form the product 2-(8-hydroxy-9H-carbazol-1-yl) acetic acid (Compound 3). Compound 3 suffered the attack from sulfate radicals, leading to the generation of compound 9. Finally, the hydroxylation of dichloroaniline (Compound 1) could yield 3,5-Dichloro-4-aminophenol (Compound 2). The generation of compound 2 was also reported in previous studies [69,76,77]. Some intermediates might suffer further degradation and be transformed to CO_2 and H_2O. As shown in Fig. S12, 16% removal efficiency of TOC (the initial TOC was 16.8 mg/L) was achieved in BFO/PMS system after 3 h. The visible light irradiation increased TOC removal efficiency from 16 to 31% (see Fig. 10).

4. Conclusions

A microwave-assisted hydrothermal method was used to synthesize BFO microspheres which can activate PMS to degrade DCF efficiently. DCF decomposition was observed to follow double-exponential decay kinetics. The influence of various parameters on DCF degradation was examined. The influence of pH ranging from 4.0 to 7.0 was not significant on DCF degradation. At pH 9.0, DCF degradation was significantly inhibited. The optimum BFO load was found to be 0.5 g L^{-1} with PMS concentration at 0.5 mM in BFO/PMS system. DCF degradation was found to follow pseudo first-order kinetics with BFO dosage

above 0.5 g L^{-1}. The degradation rates of DCF ramped up linearly with the increase of PMS concentration from 0.1 to 0.5 mM when BFO dosage was fixed at 0.5 g L^{-1}. The irradiation of visible light promoted the degradation of DCF in BFO/PMS system. Nine intermediates were identified during DCF degradation in both Vis/BFO/PMS and BFO/PMS systems. In addition, the as-prepared BFO microspheres exhibited high stability within a wide pH range. No bismuth and iron leaching were observed with pH above 4.0. These experimental results indicate the as-prepared BFO is superior to other perovskites in terms of metal ions leaching. The high stability of the as-synthesized BFO may be attributed to the microsphere morphology. The recycle tests confirmed the good reusability of BFO in both BFO/PMS and Vis/BFO/PMS systems. Decarboxylation, hydroxylation, C-N bond cleavage and intramolecular ring closure are believed to be involved in DCF degradation. Visible light irradiation also increased TOC removal efficiency during DCF degradation.

Acknowledgements

This work was financially supported by National Natural Science Foundation of China (No. 41877480) and Shaanxi Natural Science Foundation, China (No. 2017JM5074).

Appendix A. Supplementary material

Supplementary data to this article can be found online at https://doi.org/10.1016/j.seppur.2019.115967.

References

[1] J. Xu, Y. Li, B. Yuan, C. Shen, M. Fu, H. Cui, W. Sun, Large scale preparation of Cu-doped α-FeOOH nanoflowers and their photo-Fenton-like catalytic degradation of diclofenac sodium, Chem. Eng. J. 291 (2016) 174–183.
[2] F. Sacher, F.T. Lang, H.J. Brauch, I. Blankenhorn, Pharmaceuticals in groundwaters - analytical methods and results of a monitoring program in Baden-Wurttemberg, Germany, J. Chromatogr. A 938 (2001) 199–210.
[3] M. Rabiet, A. Togola, F. Brissaud, J.L. Seidel, H. Budzinski, F. Elbaz-Poulichet, Consequences of treated water recycling as regards pharmaceuticals and drugs in surface and ground waters of a medium-sized Mediterranean catchment, Environ. Sci. Technol. 40 (2006) 5282–5288.
[4] U. Jux, R.M. Baginski, H.G. Arnold, M. Kronke, P.N. Seng, Detection of pharmaceutical contaminations of river, pond, and tap water from Cologne (Germany) and surroundings, Int. J. Hyg. Environ. Heal. 205 (2002) 393–398.
[5] K.V. Thomas, M.J. Hilton, The occurrence of selected human pharmaceutical compounds in UK estuaries, Mar. Pollut. Bull. 49 (2004) 436–444.
[6] Q.W. Bu, B. Wang, J. Huang, S.B. Deng, G. Yu, Pharmaceuticals and personal care products in the aquatic environment in China: a review, J. Hazard. Mater. 262 (2013) 189–211.
[7] F. Groner, C. Hohne, W. Kleiner, W. Kloas, Chronic diclofenac exposure affects gill integrity and pituitary gene expression and displays estrogenic activity in nile tilapia (Oreochromis niloticus), Chemosphere 166 (2017) 473–481.
[8] R. Freitas, F. Coppola, S. Costa, C. Pretti, L. Intorre, V. Meucci, A. Soares, M. Sole, The influence of temperature on the effects induced by Triclosan and Diclofenac in mussels, Sci. Total Environ. 663 (2019) 992–999.
[9] K. Fent, A.A. Weston, D. Caminada, Ecotoxicology of human pharmaceuticals, Aquat. Toxicol. 76 (2006) 122–159.
[10] M.M. Sein, M. Zedda, J. Tuerk, T.C. Schmidt, A. Golloch, C. von Sonntao, Oxidation of diclofenac with ozone in aqueous solution, Environ. Sci. Technol. 42 (2008) 6656–6662.
[11] I. Michael, A. Achilleos, D. Lambropoulou, V.O. Torrens, S. Pérez, M. Petrović, D. Barceló, D. Fatta-Kassinos, Proposed transformation pathway and evolution profile of diclofenac and ibuprofen transformation products during (sono)photocatalysis, Appl. Catal., B 147 (2014) 1015–1027.
[12] K.H. Hama Aziz, H. Miessner, S. Mueller, D. Kalass, D. Moeller, I. Khorshid, M.A.M. Rashid, Degradation of pharmaceutical diclofenac and ibuprofen in aqueous solution, a direct comparison of ozonation, photocatalysis, and non-thermal plasma, Chem. Eng. J. 313 (2017) 1033–1041.
[13] V. Naddeo, V. Belgiorno, D. Kassinos, D. Mantzavinos, S. Meric, Ultrasonic degradation, mineralization and detoxification of diclofenac in water: optimization of operating parameters, Ultrason. Sonochem. 17 (2010) 179–185.
[14] D. Liu, J.Q. Wang, J. Zhou, Q.H. Xi, X. Li, E. Nie, X.Q. Piao, Z. Sun, Fabricating I doped TiO_2 photoelectrode for the degradation of diclofenac: performance and mechanism study, Chem. Eng. J. 369 (2019) 968–978.
[15] R. Homlok, E. Takacs, L. Wojnarovits, Elimination of diclofenac from water using irradiation technology, Chemosphere 85 (2011) 603–608.
[16] P. Nfodzo, H. Choi, Sulfate radicals destroy pharmaceuticals and personal care products, Environ. Eng. Sci. 28 (2011) 605–609.
[17] J. Sharma, I.M. Mishra, D.D. Dionysiou, V. Kumar, Oxidative removal of bisphenol A by UV-C/peroxymonosulfate (PMS): kinetics, influence of co-existing chemicals and degradation pathway, Chem. Eng. J. 276 (2015) 193–204.
[18] Y.C. Lee, S.L. Lo, J. Kuo, C.P. Huang, Promoted degradation of perfluorooctanic acid by persulfate when adding activated carbon, J. Hazard. Mater. 261 (2013) 463–469.
[19] T. Olmez-Hanci, I. Arslan-Alaton, Comparison of sulfate and hydroxyl radical based advanced oxidation of phenol, Chem. Eng. J. 224 (2013) 10–16.
[20] W.-D. Oh, Z. Dong, T.-T. Lim, Generation of sulfate radical through heterogeneous catalysis for organic contaminants removal: current development, challenges and prospects, Appl. Catal., B 194 (2016) 169–201.
[21] X. Chen, J. Chen, X. Qiao, D. Wang, X. Cai, Performance of nano-Co_3O_4/peroxymonosulfate system: kinetics and mechanism study using Acid Orange 7 as a model compound, Appl. Catal., B 80 (2008) 116–121.
[22] E. Grabowska, Selected perovskite oxides: characterization, preparation and photocatalytic properties—a review, Appl. Catal., B 186 (2016) 97–126.
[23] J. Zhu, H. Li, L. Zhong, P. Xiao, X. Xu, X. Yang, Z. Zhao, J. Li, Perovskite oxides: preparation, characterizations, and applications in heterogeneous catalysis, ACS Catal. 4 (2014) 2917–2940.
[24] X.G. Duan, C. Su, J. Miao, Y.J. Zhong, Z.P. Shao, S.B. Wang, H.Q. Sun, Insights into perovskite-catalyzed peroxymonosulfate activation: maneuverable cobalt sites for promoted evolution of sulfate radicals, Appl. Catal. B-Environ. 220 (2018) 626–634.
[25] Y.F. Rao, Y.F. Zhang, F.M. Han, H.C. Guo, Y. Huang, R.Y. Li, F. Qi, J. Ma, Heterogeneous activation of peroxymonosulfate by $LaFeO_3$ for diclofenac degradation: DFT-assisted mechanistic study and degradation pathways, Chem. Eng. J. 352 (2018) 601–611.
[26] H.X. Zhang, S. Cheng, B. Li, X.W. Cheng, Q.F. Cheng, Fabrication of magnetic Co/$BiFeO_3$ composite and its advanced treatment of pharmaceutical waste water by activation of peroxysulphate, Sep. Purif. Technol. 202 (2018) 242–247.
[27] W. Luo, L.H. Zhu, N. Wang, H.Q. Tang, M.J. Cao, Y.B. She, Efficient removal of organic pollutants with magnetic nanoscaled $BiFeO_3$ as a reusable heterogeneous Fenton-like catalyst, Environ. Sci. Technol. 44 (2010) 1786–1791.
[28] Y.F. Jia, C.J. Wu, D.H. Kim, B.W. Lee, S.J. Rhee, Y.C. Park, C.S. Kim, Q.J. Wang, C.L. Liu, Nitrogen doped $BiFeO_3$ with enhanced magnetic properties and photo-Fenton catalytic activity for degradation of bisphenol A under visible light, Chem. Eng. J. 337 (2018) 709–721.
[29] N. Wang, L.H. Zhu, M. Lei, Y.B. She, M.J. Cao, H.Q. Tang, Ligand-induced drastic enhancement of catalytic activity of nano-$BiFeO_3$ for oxidative degradation of bisphenol A, ACS Catal. 1 (2011) 1193–1202.
[30] F.L. Chi, B. Song, B. Yang, Y.H. Lv, S.L. Ran, Q.S. Huo, Activation of peroxymonosulfate by $BiFeO_3$ microspheres under visible light irradiation for decomposition of organic pollutants, RSC Adv. 5 (2015) 67412–67417.
[31] T. Soltani, B.K. Lee, Improving heterogeneous photo-Fenton catalytic degradation of toluene under visible light irradiation through Ba-doping in $BiFeO_3$ nanoparticles, J. Mol. Catal. A-Chem. 425 (2016) 199–207.
[32] T. Soltani, B.K. Lee, Enhanced formation of sulfate radicals by metal-doped $BiFeO_3$ under visible light for improving photo-Fenton catalytic degradation of 2-chlorophenol, Chem. Eng. J. 313 (2017) 1258–1268.
[33] I. Hussain, Y.Q. Zhang, M.Y. Li, S.B. Huang, W. Hayat, L.M. He, X.D. Du, G.Q. Liu, M.M. Du, Heterogeneously degradation of aniline in aqueous solution using persulfate catalyzed by magnetic $BiFeO_3$ nanoparticles, Catal. Today 310 (2018) 130–140.
[34] K. Rusevova, R. Koferstein, M. Rosell, H.H. Richnow, F.D. Kopinke, A. Georgi, $LaFeO_3$ and $BiFeO_3$ perovskites as nanocatalysts for contaminant degradation in heterogeneous Fenton-like reactions, Chem. Eng. J. 239 (2014) 322–331.
[35] Y.F. Rao, D. Xue, H.M. Pan, J.T. Feng, Y.J. Li, Degradation of ibuprofen by a synergistic UV/Fe(III)/Oxone process, Chem. Eng. J. 283 (2016) 65–75.
[36] F. Niu, D. Chen, L.S. Qin, T. Gao, N. Zhang, S. Wang, Z. Chen, J.Y. Wang, X.G. Sun, Y.X. Huang, Synthesis of Pt/$BiFeO_3$ heterostructured photocatalysts for highly efficient visible-light photocatalytic performances, Sol. Energy Mater. Sol. C 143 (2015) 386–396.
[37] J. Yin, G.Z. Liao, J.L. Zhou, C.M. Huang, Y. Ling, P. Lu, L.S. Li, High performance of magnetic $BiFeO_3$ nanoparticle-mediated photocatalytic ozonation for wastewater decontamination, Sep. Purif. Technol. 168 (2016) 134–140.
[38] M.J. Chen, J. Yao, Y. Huang, H. Gong, W. Chu, Enhanced photocatalytic degradation of ciprofloxacin over Bi_2O_3/$(BiO)_{(2)}CO_3$ heterojunctions: efficiency, kinetics, pathways, mechanisms and toxicity evaluation, Chem. Eng. J. 334 (2018) 453–461.
[39] T. Yamashita, P. Hayes, Analysis of XPS spectra of Fe^{2+} and Fe^{3+} ions in oxide materials, Appl. Surf. Sci. 255 (2009) 8194.
[40] D. Lebeugle, D. Colson, A. Forget, M. Viret, P. Bonville, J.F. Marucco, S. Fusil, Room-temperature coexistence of large electric polarization and magnetic order in $BiFeO_3$ single crystals, Phys. Rev. B 76 (2007).
[41] Y. Yoshida, G. Langouche, Mössbauer Spectroscopy, Springer-Verlag, Berlin Heidelberg, 2013.
[42] A. Khan, H.B. Wang, Y. Liu, A. Jawad, J. Ifthikar, Z.W. Liao, T. Wang, Z.Q. Chen, Highly efficient alpha-Mn_2O_3@alpha-MnO_2-500 nanocomposite for peroxymonosulfate activation: comprehensive investigation of manganese oxides, J. Mater Chem. A 6 (2018) 1590–1600.
[43] C. Su, X.G. Duan, J. Miao, Y.J. Zhong, W. Zhou, S.B. Wang, Z.P. Shao, Mixed conducting perovskite materials as superior catalysts for fast aqueous-phase advanced oxidation: a mechanistic study, ACS Catal. 7 (2017) 388–397.
[44] J. Flanagan, W.P. Griffith, A.C. Skapski, The active principle of caros acid, HSO_5^-X-Ray crystal structure of KHSO5.H2O, J. Chem. Soc. Chem. Commun. (1984) 1574–1575.

[45] A.R. Negri, G. Jimenez, R.T. Hill, R.C. Francis, Caroate delignification Part 4: the generation and role of hydroxyl radicals, TAPPI J. 81 (1998) 241–246.
[46] P. Maruthamuthu, P. Neta, Radiolytic chain decomposition of peroxomonophosphoric and peroxomonosulfuric acids, J. Phys. Chem. 81 (1977) 937–940.
[47] M. Descostes, P. Vitorge, C. Beaucaire, Pyrite dissolution in acidic media, Geochim. Cosmochim. Ac. 68 (2004) 4559–4569.
[48] C.D. Qi, X.T. Liu, J. Ma, C.Y. Lin, X.W. Li, H.J. Zhang, Activation of peroxymonosulfate by base: implications for the degradation of organic pollutants, Chemosphere 151 (2016) 280–288.
[49] G. Fang, W. Wu, C. Liu, D.D. Dionysiou, Y. Deng, D. Zhou, Activation of persulfate with vanadium species for PCBs degradation: a mechanistic study, Appl. Catal., B 202 (2017) 1–11.
[50] G.S. Timmins, K.J. Liu, E.J.H. Bechara, Y. Kotake, H.M. Swartz, Trapping of free radicals with direct in vivo EPR detection: a comparison of 5,5-dimethyl-1-pyrroline-N-oxide and 5-diethoxyphosphoryl-5-methyl-1-pyrroline-N-oxide as spin traps for $HO^{\cdot}$ and SO_4, Free Rad. Bio. Med. 27 (1999) 329–333.
[51] X.Z. Li, F.B. Li, Study of Au/Au^{3+}-TiO_2 photocatalysts toward visible photooxidation for water and wastewater treatment, Environ. Sci. Technol. 35 (2001) 2381–2387.
[52] P. Neta, R.E. Huie, A.B. Ross, Rate constants for reactions of inorganic radicals in aqueous solution, J. Phys. Chem. Ref. Data 17 (1988) 1027–1284.
[53] M.M. Ahmed, S. Barbati, P. Doumenq, S. Chiron, Sulfate radical anion oxidation of diclofenac and sulfamethoxazole for water decontamination, Chem. Eng. J. 197 (2012) 440–447.
[54] H. Yu, E. Nie, J. Xu, S.W. Yan, W.J. Cooper, W.H. Song, Degradation of diclofenac by advanced oxidation and reduction processes: kinetic studies, degradation pathways and toxicity assessments, Water Res. 47 (2013) 1909–1918.
[55] I.Y. Kim, M.K. Kim, Y. Yoon, J.K. Im, K.D. Zoh, Kinetics and degradation mechanism of clofibric acid and diclofenac in UV photolysis and UV/H_2O_2 reaction, Desalin. Water Treat. 52 (2014) 6211–6218.
[56] Y. Xu, J. Ai, H. Zhang, The mechanism of degradation of bisphenol A using the magnetically separable $CuFe_2O_4$/peroxymonosulfate heterogeneous oxidation process, J. Hazard. Mater. 309 (2016) 87–96.
[57] T. Zhang, H.B. Zhu, J.P. Croue, Production of sulfate radical from peroxymonosulfate induced by a magnetically separable $CuFe_2O_4$ spinel in water: efficiency, stability, and mechanism, Environ. Sci. Technol. 47 (2013) 2784–2791.
[58] P.P. Gao, X.K. Tian, Y.L. Nie, C. Yang, Z.X. Zhou, Y.X. Wang, Promoted peroxymonosulfate activation into singlet oxygen over perovskite for ofloxacin degradation by controlling the oxygen defect concentration, Chem. Eng. J. 359 (2019) 828–839.
[59] F.R. Guo, K.J. Wang, J.H. Lu, J.C. Chen, X.W. Dong, D.S. Xia, A.Q. Zhang, Q. Wang, Activation of peroxymonosulfate by magnetic carbon supported Prussian blue nanocomposite for the degradation of organic contaminants with singlet oxygen and superoxide radicals, Chemosphere 218 (2019) 1071–1081.
[60] S.S. Yang, P.X. Wu, J.Q. Liu, M.Q. Chen, Z. Ahmed, N.W. Zhu, Efficient removal of bisphenol A by superoxide radical and singlet oxygen generated from peroxymonosulfate activated with Fe-0-montmorillonite, Chem. Eng. J. 350 (2018) 484–495.
[61] P.H. Shao, J.Y. Tian, F. Yang, X.G. Duan, S.S. Gao, W.X. Shi, X.B. Luo, F.Y. Cui, S.L. Luo, S.B. Wang, Identification and regulation of active sites on nanodiamonds: establishing a highly efficient catalytic system for oxidation of organic contaminants, Adv. Funct. Mater. 28 (2018) 1705295.
[62] R.E. Huie, C.L. Clifton, N. Altstein, A pulse radiolysis and flash photolysis study of the radicals SO_2, SO_3, SO_4 AND SO_5, Radiat. Phys. Chem. 33 (1989) 361–370.
[63] H. Lee, H.J. Lee, J. Jeong, J. Lee, N.B. Park, C. Lee, Activation of persulfates by carbon nanotubes: oxidation of organic compounds by nonradical mechanism, Chem. Eng. J. 266 (2015) 28–33.
[64] E.T. Yun, G.H. Moon, H. Lee, T.H. Jeon, C. Lee, W. Choi, J. Lee, Oxidation of organic pollutants by peroxymonosulfate activated with low-temperature-modified nanodiamonds: understanding the reaction kinetics and mechanism, Appl. Catal. B-Environ. 237 (2018) 432–441.
[65] T. Zhang, Y. Chen, Y.R. Wang, J. Le Roux, Y. Yang, J.P. Croue, Efficient peroxydisulfate activation process not relying on sulfate radical generation for water pollutant degradation, Environ. Sci. Technol. 48 (2014) 5868–5875.
[66] J.Y. Wang, F.M. Han, Y.F. Rao, T.F. Hu, Y. Huang, J.J. Cao, S.C. Lee, Visible-light-driven nitrogen-doped carbon quantum dots/$CaTiO_3$ composite catalyst with enhanced NO adsorption for NO removal, Ind. Eng. Chem. Res. 57 (2018) 10226–10233.
[67] L.A. Perez-Estrada, S. Malato, W. Gernjak, A. Aguera, E.M. Thurman, I. Ferrer, A.R. Fernandez-Alba, Photo-fenton degradation of diclofenac: identification of main intermediates and degradation pathway, Environ. Sci. Technol. 39 (2005) 8300–8306.
[68] X. Cheng, P. Wang, H. Liu, Visible-light-driven photoelectrocatalytic degradation of diclofenac by N, S-TiO_2 /TiO_2 NTs photoelectrode: performance and mechanism study, J. Environ. Chem. Eng. 3 (2015) 1713–1719.
[69] J. Gou, Q. Ma, Y. Cui, X. Deng, H. Zhang, X. Cheng, X. Li, M. Xie, Q. Cheng, H. Liu, Visible light photocatalytic removal performance and mechanism of diclofenac degradation by Ag_3PO_4 sub-microcrystals through response surface methodology, J. Ind. Eng. Chem. 49 (2017) 112–121.
[70] H. Cheng, D. Song, H. Liu, J. Qu, Permanganate oxidation of diclofenac: the pH-dependent reaction kinetics and a ring-opening mechanism, Chemosphere 136 (2015) 297–304.
[71] S. Salaeh, D. Juretic Perisic, M. Biosic, H. Kusic, S. Babic, U. Lavrencic Stangar, D.D. Dionysiou, A. Loncaric Bozic, Diclofenac removal by simulated solar assisted photocatalysis using TiO_2 -based zeolite catalyst; mechanisms, pathways and environmental aspects, Chem. Eng. J. 304 (2016) 289–302.
[72] J. Li, T. Zhang, M. Ye, Heterogeneous oxidation of diclofenac in the presence of α-MnO_2 nanorods: influence of operating factors and mechanism, Water Sci. Technol. 71 (2015) 1340.
[73] L. Lonappan, T. Rouissi, M.A. Laadila, S.K. Brar, L. Hernandez Galan, M. Verma, R.Y. Surampalli, Agro-industrial-produced laccase for degradation of diclofenac and identification of transformation products, ACS Sustain. Chem. Eng. 5 (2017) 5772–5781.
[74] L.J. Xu, W. Chu, L. Gan, Environmental application of graphene-based $CoFe_2O_4$ as an activator of peroxymonosulfate for the degradation of a plasticizer, Chem. Eng. J. 263 (2015) 435–443.
[75] X. Lu, Y.S. Shao, N.Y. Gao, J.X. Chen, Y.S. Zhang, H.M. Xiang, Y.L. Guo, Degradation of diclofenac by UV-activated persulfate process: kinetic studies, degradation pathways and toxicity assessments, Ecotox. Environ. Safe. 141 (2017) 139–147.
[76] S. Chong, G.M. Zhang, N. Zhang, Y.C. Liu, T. Huang, H.Z. Chang, Diclofenac degradation in water by FeCeOx catalyzed H_2O_2: influencing factors, mechanism and pathways, J. Hazard. Mater. 334 (2017) 150–159.
[77] S.A. Cinar, A. Ziylan-Yavas, S. Catak, N.H. Ince, V. Aviyente, Hydroxyl radical-mediated degradation of diclofenac revisited: a computational approach to assessment of reaction mechanisms and by-products, Environ. Sci. Pollut. R. 24 (2017) 18458–18469.